THE JOURNAL OF PHYSICAL CHEMISTRY B
A JOURNAL OF THE AMERICAN CHEMICAL SOCIETY

pubs.acs.org/JPCB

Article

Ionic Cooperativity between Lysine and Potassium in the Lysine Riboswitch: Single-Molecule Kinetic and Thermodynamic Studies

Andrea Marton Menendez and David J. Nesbitt*

Cite This: *J. Phys. Chem. B* 2023, 127, 2430−2440

Read Online

ACCESS | Metrics & More | Article Recommendations | Supporting Information

ABSTRACT: Functionality in many biological systems, including proteins and nucleic acid structures, including protein and nucleic acid riboswitch structures, can depend on cooperative kinetic behavior between multiple small molecule ligands. In this work, single-molecule FRET data on the *Bacillus subtilis* lysine riboswitch reveals that affinity for the cognate lysine ligand increases significantly with K^+, providing evidence for synergism between lysine/K^+ binding to the aptamer and successful folding of the riboswitch. To describe/interpret this more complex kinetic scenario, we explore the conventional 4-state ("square") model for aptamer binding as a function of K^+. Extension into this additional dimension generates a novel "cube" model for riboswitch folding dynamics with respect to lysine/K^+ binding, revealing that riboswitch folding (k_{fold}) and unfolding (k_{unfold}) rate constants increase and decrease dramatically with K^+, respectively. Furthermore, temperature-dependent single-molecule kinetic studies indicate that the presence of K^+ entropically enhances the transition state barrier to folding but partially compensates for this by increasing the overall exothermicity for lysine binding. We rationalize this behavior as evidence that K^+ facilitates hydrogen bonding between the negatively charged carboxyl group of lysine and the RNA, increasing structural rigidity and lowering entropy in the binding pocket. Finally, we explore the effects of cation size with Na^+ and Cs^+ studies to demonstrate that K^+ is optimally suited for bridging interactions between lysine and the riboswitch aptamer domain. Regulation of lysine production and transport, dictated by the riboswitch's ability to recognize and bind lysine, is therefore intimately tied to the presence of K^+ in the binding pocket and is strongly modulated by local cation conditions. The results suggest an increase in lysine riboswitch functionality by sensitivity to additional species in the cellular riboswitch environment.

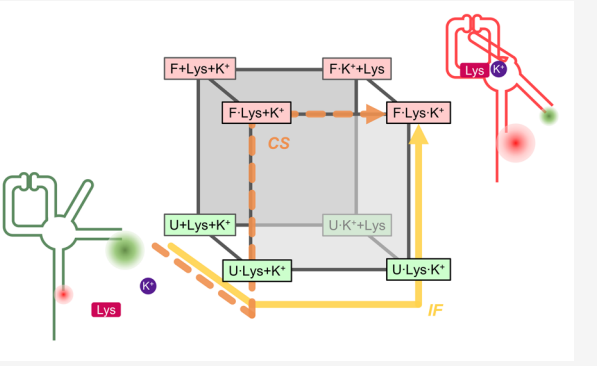

1. INTRODUCTION

Riboswitches are highly functional RNA motifs, consisting of an aptamer and an expression platform typically found in the 5′ untranslated region and used to regulate downstream genes.[1−4] The aptamer domain of a riboswitch detects and binds a target ligand, which in turn generates structural modifications in the expression platform that dictates whether the downstream gene is translated and/or transcribed.[5,6] Riboswitches have been identified that bind to a wide variety of ligands, including metal cations, such as the manganese[7] and nickel/cobalt[8] riboswitches, amino acids and cofactors (e.g., the guanine[9] and SAM family[10] of riboswitches), and even simple anions as in the fluoride riboswitch.[11] Their ability to distinguish between similar ligand structures and chemistry[12,13] makes riboswitches highly effective bacterial[14] and eukaryotic[15,16] gene regulators, which in turn makes them attractive targets for antimicrobial therapeutics[17,18] and as engineered molecular sensors.[19,20] Furthermore, structures with multiple binding sites, like those found in some TPP,[21] cyclic di-AMP,[22] and in SAM[23] riboswitches, introduce more exotic gene regulation strategies. For example, such multisite sequential aptamer/expression platform units can even function independently to perform logic operations, such as NOR gate activity in the TPP riboswitch.[4] The glycine riboswitch has a particularly interesting tandem architecture (two glycine aptamers built into a single expression platform), which demonstrates cooperativity between the two glycine molecules it binds.[24−26] Cooperative behavior between ligands and small molecules or ions in riboswitches has also been found, especially for systems where magnesium contributes to riboswitch folding,[27,28] often by an increase in the ligand binding rates or affinities.

Cooperativity and allosteric modulation exist in a huge range of systems with multiple binding sites such as proteins,[29−32] ribozymes,[33] nucleic acid structures,[34,35] and bio-inspired catalysts,[36−38] where binding a first ligand impacts the ligand

Received: January 11, 2023
Revised: February 21, 2023
Published: March 14, 2023

https://doi.org/10.1021/acs.jpcb.3c00245
J. Phys. Chem. B 2023, 127, 2430−2440

binding affinity for other sites. The ligands involved can be identical in all sites, as in the binding of four O_2 molecules to hemoglobin,[39] or be different species to achieve separate functions, as in small molecule-induced conformational changes for opening/closing catalytic metal sites to their intended targets.[40] Indeed, mechanistic interpretations of allostery often rely on structural reorganization upon the first ligand binding event that unblocks other sites with biomolecular "hinges" or equivalent features, modulation of the electrostatic environment, or even changes in conformer populations available to the biomolecule containing the binding site.[31,41,42] This diversity in cooperativity and allostery has given rise to additional powerful applications in drug discovery, with options for targets that avoid an active site or exploit allosterically controlled interactions.[43,44] Synthetic structures have been developed that take advantage of such cooperative behavior according to schemes that construct new systems based on rational design,[43,45] previous knowledge of the function and structure of other biomolecules, or directed evolution,[38] in which sections of enzymes and ribozymes are engineered to introduce new functionalities.

In the present study, we explore and exploit principles of cooperativity to investigate the *Bacillus subtilis* lysine riboswitch, which regulates genes involved in the production and transport of lysine.[3,5,46] The aptamer portion of the riboswitch contains five helices that envelop a lysine molecule in the central junction, as shown in Figure 1a.[47] The riboswitch

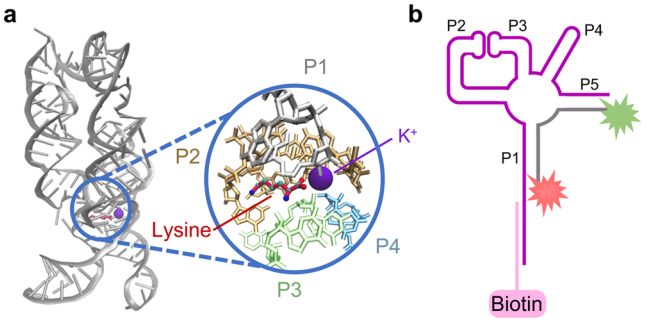

Figure 1. Diagrams of the lysine riboswitch: (a) the crystal structure (PDB: 3DIL) of a folded lysine riboswitch; the inset shows K^+ and lysine bound within the binding pocket. (b) Schematic of the modified construct with Cy3 (green burst) and Cy5 (red burst) labeling, and biotinylation for single-molecule TIRF studies.

is able to discriminate against lysine analogues such as S-(2-aminoethyl)-L-cysteine and L-4-oxalysine by a 10−100-fold preference for lysine in in vitro assays,[48] with recognition of lysine based on stabilizing hydrogen bonds between the ammonium group and the RNA as well as steric constraints in the binding pocket that exclude molecules of different sizes. Although some tertiary structure exists before lysine is bound (e.g., the P2−P3 kissing-loop interaction),[49,50] aptamer binding triggers additional tertiary changes to the riboswitch, in particular shortening of the P1−P5 distance which, with the help of distance-dependent donor/acceptor FRET labels, can fluorescently sense folding of the riboswitch.[51−53] The riboswitch folding mechanism has been shown in previous studies to rely on lysine binding as an essential prerequisite to subsequent conformational change.[51] In the context of such an induced-fit (i.e., "bind-then-fold", IF) pathway, the unfolded riboswitch (U) first must bind with lysine (Lys) and only then can undergo structural rearrangement to the correctly folded state (F): U + Lys ⇌ U·Lys ⇌ F·Lys. Even more relevantly, riboswitch folding is known from previous studies to be penalized by loss of entropy and yet compensated by enthalpic release,[54] as lysine forms several hydrogen bonds to internal contacts in the binding pocket[48] but is highly restricted once bound. However, although the majority of the entropic cost to folding along the U → TS → F pathway takes place before the transition state (TS), only <50% of the overall folding exothermicity is released by this point. Such a mechanistic delay between entropic penalty and enthalpic reward can thus result in large transition state barriers ($\Delta G^{\ddagger} > 0$) despite relatively small changes in the overall free energy for folding.[54]

The position of the potassium ion between the carboxylic acid and the riboswitch binding pocket (see Figure 1a insert) indicates that it most likely mediates additional bridging interactions between the negatively charged carboxyl end of lysine and the negatively charged RNA backbone. As such, potassium is predicted to stabilize the lysine-bound riboswitch[48] and create conditions that favor the folded state. Though far less biologically abundant, studies investigating alternative cation mediators reveal that K^+ can be replaced by Cs^+ and Tl^+ ions but not by Na^+ or Mn^{2+}.[48] This suggests size- and charge-dependent cationic preferences to facilitate coordinating bonds in the riboswitch and consequently that the riboswitch specificity for lysine may be influenced by the nature of the cation present in the binding pocket. In the context of an induced-fit (IF) model, potassium-promoted and stabilized ligand binding could therefore act cooperatively with lysine to enhance the rate of riboswitch folding and thus impact gene regulation.

To test this hypothesis, we have explored riboswitch folding/unfolding with single-molecule FRET methods (smFRET) to develop models for riboswitch folding that reveal kinetic cooperativity between lysine and K^+ ligands. In this work, we expand the conventional four-state (i.e., "square") model used in previous studies[51,55] into an extra K^+ dimension (i.e., a "cube" model), where the eight states or "vertices" now represent (i) folded (F) vs unfolded (U) riboswitch conformations with bound vs unbound (ii) potassium and (iii) lysine ligands. In addition, we also pursue these smFRET thermodynamic and kinetic studies as a function of temperature to deconstruct all free energies into enthalpic and entropic components. Because these studies are also all performed as a function of potassium concentration, this serves to highlight a surprisingly strong synergism between K^+ and the thermodynamics of lysine binding to the aptamer domain, which in analogy to more conventionally allosteric systems[24,27,31,56] reflects a simple example of "ionic cooperativity."

The structure of this paper is as follows. In Sections 3.1−3.4, we explore potassium-induced changes to riboswitch folding to reveal changes in both the folding and unfolding rates that favor the folded riboswitch state. The data allow us to propose a predominant, but not exclusive, folding pathway in which lysine first binds to the riboswitch (U + Lys → U·Lys), the riboswitch then folds (U·Lys → F·Lys), after which potassium binding occurs (F·Lys + K^+ → F·Lys·K^+) to stabilize the folded conformation. In Section 3.5, we discuss the temperature-dependent thermodynamics of folding at low and high potassium concentrations to show that K^+ increases the enthalpic benefit ($\Delta\Delta H^\circ < 0$) but also the entropic penalty to folding ($-T\Delta\Delta S^\circ > 0$). Finally, in Section 4, we consider substitution studies of both larger and smaller monovalent

https://doi.org/10.1021/acs.jpcb.3c00245
J. Phys. Chem. B 2023, 127, 2430−2440

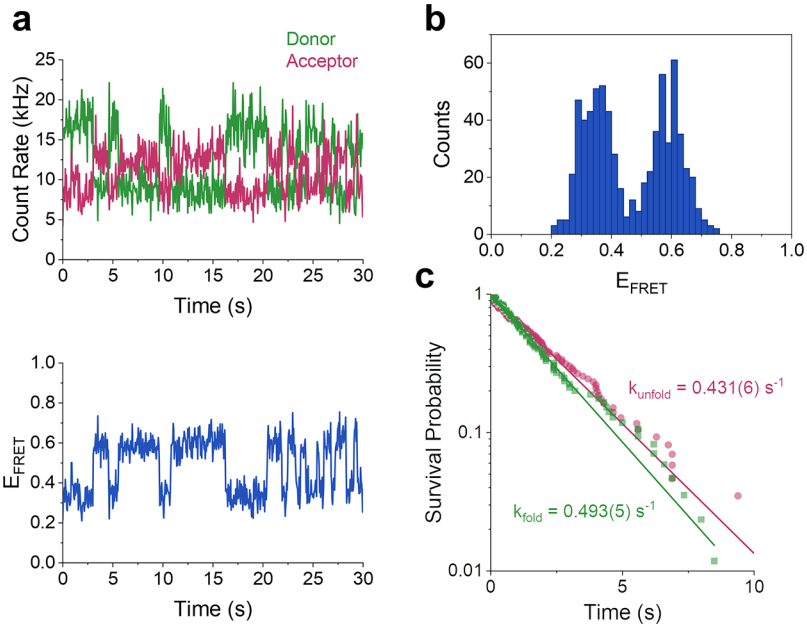

Figure 2. Sample data and analysis: (a) example time trace of single-molecule data. (Top) donor (Cy3) and acceptor (Cy5) fluorescence intensities, (bottom) FRET efficiencies. (b) Histogram of FRET efficiencies showing two FRET peaks near E_{FRET} = 0.3 and 0.6. (c) Survival probability analysis of open and closed state dwell time distributions.

cations, which indicate, in agreement with previous ensemble work, that Cs^+ promotes folding behavior while Na^+ does not. Kinetic models for Cs^+ and Na^+ substitution are presented to demonstrate that Cs^+ only binds after the riboswitch folds in a conformational selection (CS) or "fold-then-bind" pathway, while Na^+ does not appear to localize in the binding pocket and instead stabilizes the negatively charged RNA backbone in both folded/unfolded riboswitch conformations.

2. METHODS

To perform single-molecule kinetic and thermodynamic studies of lysine riboswitch folding, we use a modified, three-strand aptamer structure, as shown schematically in Figure 1b.[51,52,54] The construct includes a strand with a Cy3-Cy5 FRET pair on distal ends that form the P1 and P5 helices and a complementary biotinylated strand that anneals with an extended region of P1 such that individual molecules can be immobilized on the surface for smFRET measurements. As in other studies,[57−59] samples are prepared in glass flow cells and sequentially flushed with solutions to (i) passivate the surface, (ii) tether the RNA, and (iii) create appropriate salt, buffer, and oxygen-scavenging conditions. Briefly, glass coverslips are cleaned in a UV−ozone oven before introducing solutions of (i) bovine serum albumin (BSA) with biotinylated BSA (10% biotinylated BSA/90% unbiotinylated BSA) to coat the glass surface and create biotin-tethering sites, (ii) a streptavidin solution (0.2 mg/mL) that binds to the biotin surface sites, and (iii) the biotinylated RNA sample which attaches to free sites in the streptavidin, with each solution incubated for 10 min before the next is introduced. Finally, we flow in an imaging solution consisting of HEPES buffer, lysine, background KCl, NaCl, and $MgCl_2$ solutes at the desired concentrations and an oxygen-scavenging system (PCD, PCA, and Trolox) and seal the sample with epoxy to prevent evaporation.

We study the effects of $[K^+]$ on riboswitch folding via temperature-controlled single-molecule total internal reflection microscopy (TIRF), whereby a 532 nm diode-pumped solid-state laser is focused on the back focal plane of a high numerical aperture (NA = 1.4) microscope objective, laterally displaced from the optical axis to achieve total internal reflection and wide field illumination of the sample surface.[54,60] The resulting sample fluorescence is collected through the same objective and separated by a dichroic mirror (Chroma 645 nm LP) to sort emission photons according to donor and acceptor channels, recombined by another dichroic mirror with a horizontal offset and imaged onto a PI I-PentaMAX 512-EFT CCD camera. Movies of the folding kinetics are analyzed with custom LabWindows/CVI software, where collocated donor and acceptor emissions from the same biomolecule are used to create single-molecule fluorescence intensity trajectories (Figure 2a). Temperature control is achieved via two thermoelectric coolers, one placed on the sample and the other on the microscope objective itself.

Emission intensity data collected in the donor (I_D) and acceptor (I_A) fluorescence channels are analyzed to extract time-dependent E_{FRET} trajectories: $E_{FRET} = I_A/(I_A + I_D)$ (see Figure 2a), which in turn distinguish between folded (F) or unfolded (U) riboswitch states. A histogram of E_{FRET} values (see Figure 2b) depicts two clearly defined peaks that correspond to the unfolded (low E_{FRET} = 0.3) and folded (high E_{FRET} = 0.6) riboswitch conformations. We set the local minimum between the two peaks as the threshold, with abrupt bin-time-limited transitions between the two E_{FRET} values denoting switching between the folded and unfolded states. Riboswitch dwell times spent in one state before switching back to the other are further analyzed to extract the folding (k_{fold}) and unfolding (k_{unfold}) rate constants, which are assumed (and empirically confirmed) to be elementary unimolecular processes.[61] Cumulative distribution functions of survival probabilities for folded and unfolded states are therefore fit to single exponential decays to determine k_{unfold} and k_{fold} rate constants, respectively (see Figure 2c). Finally, equilibrium

https://doi.org/10.1021/acs.jpcb.3c00245
J. Phys. Chem. B 2023, 127, 2430−2440

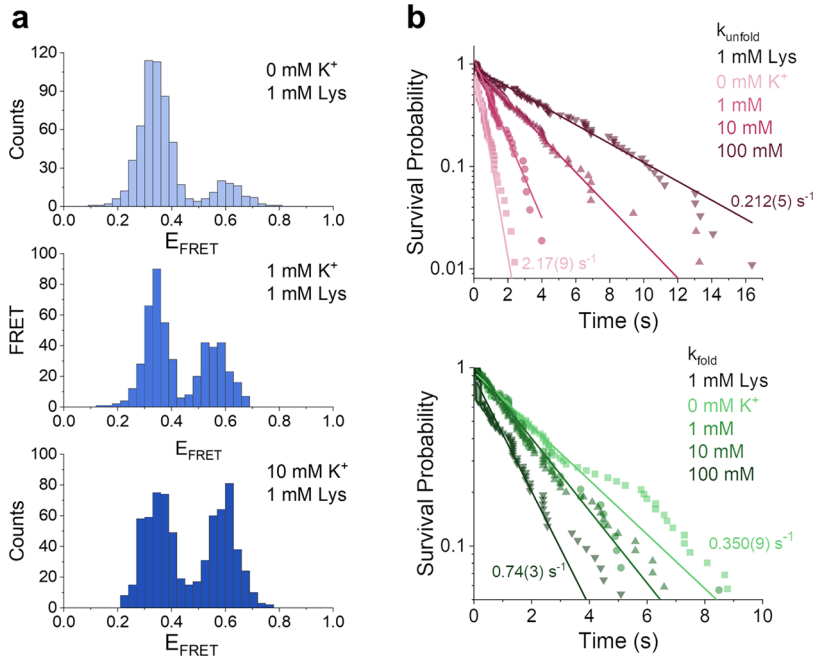

Figure 3. Equilibrium and rate constant data as a function of increasing [K+]: (a) top to bottom: histograms of FRET efficiencies at 0, 1, and 10 mM K+ demonstrate an increase in folded riboswitch population (at E_{FRET} = 0.6) and a decrease in the unfolded state (E_{FRET} = 0.3). (b) Survival probability analysis of the folded state (top right) reveals that the unfolding rate constant decreases dramatically (≈10×), while the unfolded state dwell times (bottom right) reveal a corresponding increase in the folding rate with [K+].

constants (K_{eq}) are obtained as ratios of folding to unfolding rate constants, $K_{eq} = k_{fold}/k_{unfold}$.

3. RESULTS

3.1. Potassium Increases k_{fold} and Decreases k_{unfold} to Increase K_{eq}. The potassium cation is thought to moderate repulsion between the negatively charged carboxylic acid lysine end and the riboswitch RNA backbone,[48] e.g., strengthening the bonding between lysine and the riboswitch, correctly orienting lysine within the binding pocket or via other interactions enhancing the equilibrium constant (K_{eq}) between folded and unfolded states. Indeed, we clearly see such effects in the equilibrium FRET histograms (see Figure 3a), which indicate a rapid rise in fractional time the riboswitch spends folded at higher K+ concentration. Such effects can be quantified in greater kinetic detail by analysis of survival dwell time distributions (see Figure 3b), which reveal the dramatic increase in K_{eq} to arise from a simultaneous *increase* in k_{fold} and *decrease* in k_{unfold} rate constants with potassium concentration, both of which favor the folded riboswitch. Most relevantly, we have explored this cooperative K+ enhancement of the fractional riboswitch folding on lysine. As evident in Figure 4, higher K+ concentrations significantly decrease K_D for lysine, indicating that potassium ions cause lysine to bind more tightly to the riboswitch. This suggests that potassium is a critical species in lysine-riboswitch gene regulation through stabilization of the lysine-bound state, which is in itself a prerequisite for subsequent biocompetent folding of the riboswitch.

3.2. Riboswitch Folds via an Induced-Fit (IF) Mechanism in the Absence of Potassium. With K+ and lysine identified as synergistic partners in the folding event, we turn first to lysine-promoted riboswitch folding at 0 mM K+, in accordance with the simple 4-state model illustrated schematically in Figure 5. It is worth stressing that although folded and

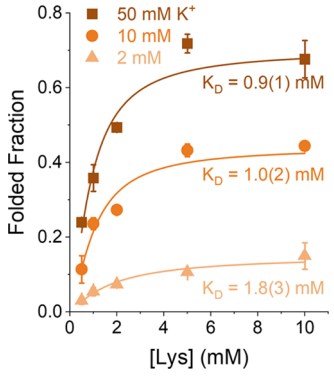

Figure 4. Hill analysis of lysine binding at [K+] = 1, 10, and 50 mM shows that the binding constant for lysine decreases with increased [K+] (results for all [K+] values available in SI Table 1).

unfolded riboswitch conformations are easily detected as high and low FRET states, respectively, the lysine-bound and unbound versions (F + Lys vs F·Lys; U + Lys vs U·Lys) are experimentally indistinguishable. However, any ambiguity between lysine-bound/unbound states can be cleanly resolved in the context of such a 4-state kinetic model by examining [Lys]-dependent changes to the observed folding (k_{fold}) or unfolding (k_{unfold}) rate constants. Specifically, previous work[S1] has shown that lysine binding occurs via an induced-fit (IF) pathway, whereby binding to the aptamer domain occurs prior to overall riboswitch folding. Such a mechanism therefore offers a simplified kinetic scenario (under [K+] = 0 conditions) in which only three states are available: (i) the unfolded, unbound state (U + Lys), (ii) the unfolded, lysine-bound state (U·Lys), and (iii) the folded, lysine-bound state (F·Lys), with all three species connected by the "counter-clockwise" (ccw) sequence U + Lys ⇌ U·Lys ⇌ F·Lys. In such a "bind-then-fold" mechanism, one expects the effective folding rate

https://doi.org/10.1021/acs.jpcb.3c00245
J. Phys. Chem. B 2023, 127, 2430−2440

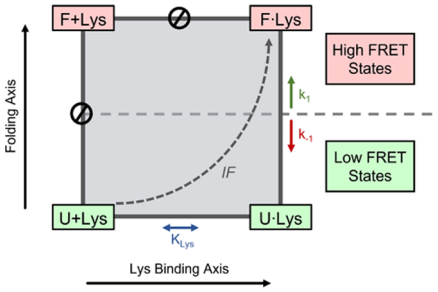

Figure 5. Four-state "square" model for lysine binding to the riboswitch. The unfolded riboswitch states are on the bottom edge of the square in green to represent their low FRET efficiencies (E_{FRET} = 0.3), while folded riboswitch states are on the top edge in red to denote their high FRET efficiencies (E_{FRET} = 0.6). Transitions between observed riboswitch/lysine states are characteristic of induced-fit folding states and are labeled with dissociation and rate constants; transitions to the unobserved state (F + Lys) are blocked.

constant to increase toward saturation with [Lys] while the unfolding rate constant remains [Lys] independent. Derivations for these and other kinetic models in section 3.3 can be found in SI sections 1−2.

$$\mathrm{U} + \mathrm{Lys} \overset{K_{Lys}}{\rightleftharpoons} \mathrm{U{\cdot}Lys} \overset{k_1}{\rightarrow} \mathrm{F{\cdot}Lys}$$

$$k_{fold} = \frac{k_1[\mathrm{Lys}]}{[\mathrm{Lys}] + K_{Lys}}$$

$$\mathrm{F{\cdot}Lys} \underset{k_{-1}}{\longrightarrow} \mathrm{U{\cdot}Lys}$$

$$k_{unfold} = k_{-1}$$

This provides valuable contrast with corresponding predictions for a conformational selection (CS) "fold-then-bind" mechanism, in which the riboswitch samples many different conformations with a specific folded state stabilized by ligand binding, U + L ⇌ F + L ⇌ FL. In such an alternative "clockwise" (cw) limit, one anticipates the effective rate constants k_{unfold} to decrease and k_{fold} to remain independent of [Lys].

$$\mathrm{U} + \mathrm{Lys} \overset{k_1}{\rightarrow} \mathrm{F} + \mathrm{Lys}$$

$$k_{fold} = k_1$$

$$\mathrm{F{\cdot}Lys} \overset{K_{Lys}}{\rightleftharpoons} \mathrm{F} + \mathrm{Lys} \overset{k_{-1}}{\longrightarrow} \mathrm{U} + \mathrm{Lys}$$

$$k_{unfold} = \frac{k_{-1}K_{Lys}}{[\mathrm{Lys}] + K_{Lys}}$$

The [K^+] = 0 mM data presented in Figure 6 is in excellent agreement with an induced-fit mechanism, with virtually zero lysine dependence in the unfolding rate but a clear [Lys]-dependent increase to saturation in the folding rate. Indeed, analysis of the smFRET trajectories for [K^+] = 0 to the induced-fit expressions yield unimolecular folding (k_1 = 3.3(5) s^{-1}, K_{Lys} = 5(2) mM) and unfolding ($k_{unfold} = k_{-1}$ = 1.32(7) s^{-1}) rate constants, which in section 3.3 below will in turn be used as a baseline reference for kinetic studies at non-zero potassium conditions.

3.3. An 8-State "Cube" Model Describes Lysine and Potassium Effects on Riboswitch Folding. The 4-state

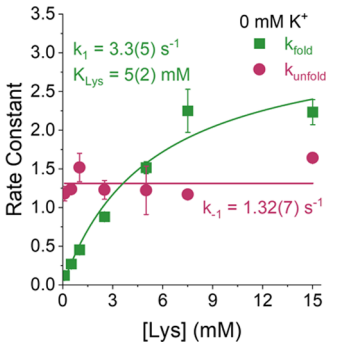

Figure 6. [Lys]-dependence of folding (green squares) and unfolding (pink circles) rate constants at 0 mM K^+. The unfolding rate constant is [Lys] independent, while the folding rate constant increases with [Lys], in agreement with an induced-fit (IF) folding mechanism.

("square") model in Figure 5 has been successfully used in multiple previous works[51,54] to describe the riboswitch folding mechanism with respect to a single ligand. However, to further understand and describe the synergistic effects between potassium and lysine on riboswitch function, we propose a higher dimensional 8-state ("cube") model, as schematically illustrated in Figure 7. This more detailed model allows us to

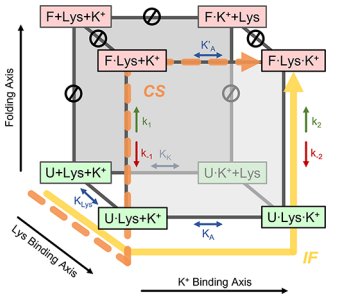

Figure 7. Eight-state "cube" model for riboswitch folding with respect to lysine and potassium binding, reflecting an expansion of the 4-state "square" model in Figure 5 along the K^+ binding axis. The left face represents [K^+] ∼0 mM conditions and is equivalent to the simplest 4-state "square" model for lysine-promoted folding. The right face reflects folding under saturated [K^+] conditions, with front and back faces comprising saturated [Lys] ∼1 mM and [Lys] ∼0 mM conditions, respectively. The four possible unfolded (U) and folded (F) riboswitch states are denoted in green (bottom face) and red (top face). Transitions between observed riboswitch states along cube edges are labeled by dissociation and rate constants, with transitions between kinetically unobserved states (e.g., F + Lys + K^+ and F·K^+ + Lys) blocked. Induced fit (IF) and conformational selection (CS) folding pathways with respect to K^+ are depicted in solid yellow and dashed red lines, respectively.

distinguish the effects on riboswitch folding by isolating potassium and lysine binding as well as folding/unfolding rate constants between all lysine and potassium-bound vs unbound states, i.e., (i) U + K^+ + Lys ⇌ F + K^+ + Lys, (ii) U·Lys + K^+ ⇌ F·Lys + K^+, (iii) U·K^+ + Lys ⇌ F·K^+ + Lys, and (iv) U·Lys·K^+ ⇌ F·Lys·K^+, each of which represents the vertical edge of a more complex kinetic "cube." Simply summarizing Figure 7, the front face captures the kinetic dependence on K^+ for lysine-bound states, with the left/right-hand faces of the cube representing [K^+] = 0 mM and saturating K^+ conditions, respectively. If we assume steady-state conditions with respect to all ion/ligand binding events, the corresponding effective

https://doi.org/10.1021/acs.jpcb.3c00245
J. Phys. Chem. B 2023, 127, 2430−2440

folding/unfolding rate constant expressions can be readily derived, with seven independent parameters required to fit each

$$k_{\text{fold}} = \frac{k_1K_KK_{Lys}[Lys] + k_2K_K[K^+][Lys] + k_3K_AK_{Lys}[K^+] + k_4K_AK_KK_{Lys}}{K_AK_KK_{Lys} + K_AK_K[Lys] + K_AK_{Lys}[K^+] + K_K[K^+][Lys]} \quad (1)$$

$$k_{\text{unfold}} = \frac{k_{-1}K'_KK'_{Lys}[Lys] + k_{-2}K'_K[K^+][Lys] + k_{-3}K'_AK'_{Lys}[K^+] + k_{-4}K'_AK'_KK'_{Lys}}{K'_AK'_KK'_{Lys} + K'_AK'_K[Lys] + K'_AK'_{Lys}[K^+] + K'_K[K^+][Lys]} \quad (2)$$

To reduce parameter correlation and improve fit quality, we simplify the above model expressions by omitting any states (i.e., "vertices") and interconnecting pathways (i.e., "edges") that violate an induced-fit folding mechanism with respect to lysine. Specifically, this excludes the folded, lysine/potassium unbound state (Figure 7, back square, upper left vertex, F + K^+ + Lys), and the folded, potassium-bound, lysine-unbound state (Figure 7, back square, upper right vertex, F·K^+ + Lys). Furthermore, we can assume that K^+ binding to the Lys-unbound state (Figure 7, back square, bottom "edge") is very weak ($K_K \gg 1$ M), as the K^+ ion is held in position by required contacts with lysine.[48] Without lysine in place, the K^+ can associate with any part of the negatively charged RNA backbone but not truly bind in the pocket, thereby removing the U·K^+ + Lys state (Figure 7, back square, bottom right vertex) from kinetic consideration. This leaves only five states of interest and a much simplified pair of expressions

$$k_{\text{fold}} = \frac{k_1K_A + k_2[K^+][Lys]}{K_AK_{Lys} + K_A[Lys] + [K^+][Lys]} \quad (3)$$

$$k_{\text{unfold}} = \frac{k_{-1}K'_A + k_{-2}[K^+]}{K'_A + [K^+]} \quad (4)$$

from which the k_{unfold} data can be fit directly to extract k_{-1} and K_A'. To most efficiently fit the k_{fold} data, we take the simplest empirical path by first fitting the potassium-free folding rate constant (k_1) separately in experiments at [K^+] = 0, as schematically shown in Figure 5 (or equivalently, the leftmost cube "face" in Figure 7). This breaking of parameter correlation allows combined least squares fit to the full set of k_{fold}, k_{unfold} data and thereby extraction of all four unimolecular folding/unfolding rate (k_1, k_{-1}, k_2, k_{-2}) and 4 dissociation (K_A, K_A', K_{Lys}, K_K) constants in eqs 3 and 4.

3.4. Both Induced-Fit (IF) and Conformational-Selection (CS) Mechanisms Available for K^+ Controlled Folding. We next investigate K^+ dependence of the riboswitch folding/unfolding rate constants for a fixed intermediate lysine concentration ([Lys] = 1 mM), data from which are plotted in Figure 8. Specifically, K^+ increases and decreases k_{fold} and k_{unfold}, respectively, with particularly dramatic effects evident at the lowest potassium ion concentrations ([K^+] ≈ 0−20 mM), above which both rate constants asymptotically approach the [K^+] saturation limits predicted from eqs 3 and 4 ($k_{\text{fold}} \approx k_2$, $k_{\text{unfold}} \approx k_{-2}$). Interestingly, the K^+ dissociation constant for the lysine-bound unfolded riboswitch (U·Lys + K^+ ⇌ U·Lys·K^+; K_A = 2.2(6) mM) is quite similar to the value for the folded riboswitch (F·Lys + K^+ ⇌ F·Lys·K^+; K_A' = 1.9(9) mM), which suggests that potassium readily binds to the riboswitch in both lysine-bound conformations. Finally, the unfolding rate constant from the previous [K^+] = 0 experiments (for which

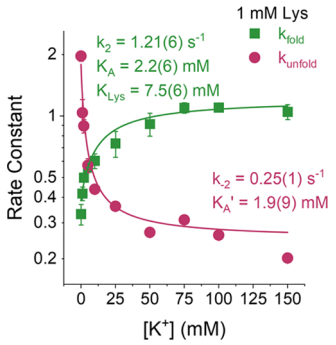

Figure 8. [K^+] dependence of riboswitch folding (green squares) and unfolding (pink circles) rate constants at [Lys] = 1 mM. The folding rate increases with [K^+], while the unfolding rate decreases considerably with [K^+], which is consistent with both induced-fit and conformational selection pathways available for K^+ binding.

$k_{\text{unfold}} \approx k_{-1}$, Figure 6) agrees with k_{-1} values obtained from cube model fits to k_{unfold} data (k_{-1} = 1.32(7) s^{-1} vs 1.8(5) s^{-1}, respectively), which provides a metric for internal consistency (the complete results are summarized in SI Table 2).

The data reveal folding out of the K^+/Lys doubly bound riboswitch (U·Lys·K^+ $\xrightarrow{k_2}$ F·Lys·K^+) to be an efficient process, providing an additional route that is 40% as fast as the K^+-unbound pathway (U·Lys + K^+ $\xrightarrow{k_1}$ F·Lys + K^+), i.e., k_2 = 1.4(4) s^{-1} vs k_1 = 3.3(5) s^{-1}, respectively. By way of contrast, the K^+/Lys doubly bound unfolding rate constant is nearly 800% slower than the *unfolding* rate constant in the absence of K^+, specifically k_{-2} = 0.25(1) s^{-1} vs k_{-1} = 1.8(5) s^{-1}, respectively. As one immediate consequence, K_{eq} for riboswitch folding under saturating [K^+] conditions is 400% that at [K^+] = 0 mM, dominated by K^+-dependent slowing of the riboswitch unfolding rate constant. More importantly, however, this constitutes clear evidence for the presence of an alternative cw ("fold-then-bind," CS) pathway (Figure 7, front face, dashed red line) for promoting riboswitch folding, but this time viewed as a function of K^+ rather than lysine as the "ligand". Characterized specifically in terms of the cube model (Figure 7), the unfolded riboswitch in the absence of K^+ can bind lysine (left face, bottom edge: U + Lys + K^+ → U·Lys + K^+) and then fold (left face, front vertical edge: U·Lys + K^+ → F·Lys + K^+), with subsequent binding of K^+ (front face, top edge: F·Lys + K^+ → F·Lys·K^+) stabilizing the F·Lys·K^+ state and preventing unfolding. Equally important, however, the data clearly reveal that the riboswitch can also fold via a ccw ("bind-then-fold," IF) pathway (Figure 7, front face, solid yellow line) triggered by K^+ binding to the unfolded construct. Geometrically summarized, the front cube face comprises kinetic competition between IF (ccw, solid yellow) and CS (cw, dashed red) folding pathways, whereas the left/right cube faces represent complementary IF (ccw, dashed red) kinetic pathways for lysine induced folding with either K^+ unbound/K^+ bound riboswitches, respectively. Taking this kinetic analysis one step further, we can also predict branching ratios characterizing the dominant K^+ folding and binding mechanism: either via the induced fit (U + Lys + K^+ ⇌ U·Lys + K^+ ⇌ U·Lys·K^+ → F·Lys·K^+) or the conformational selection (U + Lys + K^+ ⇌ U·Lys + K^+ → F·Lys + K^+ ⇌ F·Lys·K^+) path. From the least squares fitted rate and equilibrium constant results, the IF/CS branching ratios (Q) for K^+-dependent folding/binding at [Lys] = 1 mM are

https://doi.org/10.1021/acs.jpcb.3c00245
J. Phys. Chem. B 2023, 127, 2430−2440

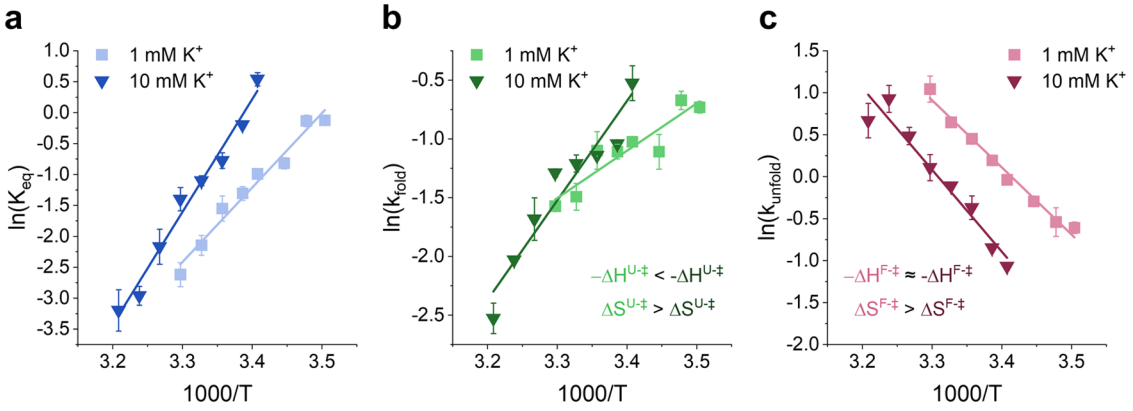

Figure 9. Temperature dependence of riboswitch folding at 1 mM K^+ (light squares) and 10 mM K^+ (dark inverted triangles). (a) The van't Hoff plot shows that the equilibrium constant increases with decreasing temperature and increasing [K^+]. (b) The Arrhenius plot for folding (green) rate constants, which increases with decreasing temperature. The fitted slope increases with [K^+], indicating $\Delta\Delta H^{U\text{-}‡} < 0$, while the intercept decreases with [K^+], signaling $\Delta\Delta S^{U\text{-}‡} < 0$. (c) Unfolding data (pink) reveal that both rate constants and intercepts decrease with [K^+], but exhibit similar Arrhenius slopes at 1 and 10 mM K^+. This implies greater entropic penalty ($\Delta\Delta S^{F\text{-}‡} < 0$) at higher [$K^+$] and yet similar enthalpic changes ($\Delta\Delta H^{F\text{-}‡} \approx 0$) for the two [$K^+$] conditions, respectively.

$$Q_{IF} = (k_2/K_A)(k_1/K'_A + k_2/K_A) = 27\%$$

$$Q_{CS} = (k_1/K'_A)(k_1/K'_A + k_2/K_A) = 73\%$$

Thus, parallel contributions from both K^+-induced "fold-then-bind" (CS) and "bind-then-fold" (IF) pathways for the lysine riboswitch prove to be quite important.

3.5. Temperature Studies: Extracting Δ*H* and Δ*S* for K^+/Lysine-Dependent Folding. Cooperative ligand binding in biomolecules can impact overall thermodynamic parameters in a way that provides additional insights into the dynamics. With this as a goal, we have exploited van't Hoff analysis to study temperature-dependent[57,62] folding/unfolding equilibrium behavior

$$K_{eq} = \exp(-\Delta G^\circ/k_B T) \tag{5}$$

$$\ln(K_{eq}) = -(\Delta H^\circ/k_B)(1/T) + \Delta S^\circ/k_B \tag{6}$$

to further probe for K^+/lysine cooperative kinetics in the riboswitch binding pocket. From the standard van't Hoff expression, slopes from a linear fit of $\ln(K_{eq})$ vs $1/k_BT$ yield enthalpic information ($-\Delta H^\circ$), while the intercepts characterize the entropic change ($\Delta S^\circ/k_B$). As evident from Figure 9a, the positive slopes correspond to the exothermic folding of the riboswitch, while the negative intercepts indicate increasing order in the folded state. Furthermore, both enthalpic and entropic components are significantly impacted by K^+ concentration, signaling an increase in folding exothermicity: $-\Delta H^\circ$(1 mM K^+) < $-\Delta H^\circ$(10 mM K^+), and a decrease in the folded state entropy: ΔS°(1 mM K^+) > ΔS°(10 mM K^+) with increasing [K^+].

There is also valuable information on the temperature dependence of the folding/unfolding rate constants themselves (see Figure 9b,c) beyond obtaining overall thermodynamic changes (ΔG°, ΔH°, ΔS°) from the equilibrium folding data. In particular, such temperature-dependent rate constant studies provide thermodynamic information on the transition state (TS) barrier to folding under specific [Lys] and [K^+] conditions, according to Kramers analysis[60,63]

$$\ln(k_{fold(unfold)}) = (-\Delta G^‡)/k_B T - \ln(\kappa\upsilon) = -\Delta H^‡/k_B T + \Delta S^‡/k_B - \ln(\kappa\upsilon) \tag{7}$$

for which the slopes quantify forward/reverse enthalpy release ($-\Delta H^‡$) between unfolded/folded states and the transition state. Similarly, the intercepts report on the entropic properties of the transition state, where the additional $\kappa\nu_0$ term in Eyring and Kramers theory corresponds to classical attempt frequency (ν_0) × transmission coefficient (κ) over the transition state barrier. This product of attempt frequency with transmission is not known *a priori* but is often taken to be in the 10^6–10^8 s^{-1} range for conformational transformation in large biomolecules,[64] with higher values (10^8–10^{12} s^{-1} range) for progressively smaller polyatomic species. However, as entropic changes upon reaching the transition state are only logarithmically related to the attempt frequency, order of magnitude changes in ($\kappa\nu_0$) correspond to only small (k_B scale) shifts in the ($\Delta S^‡$) transition state entropy. Furthermore, any differential metabolite-induced changes in $\Delta S^‡$ (i.e., $\Delta\Delta S^‡$) as a function of K^+ are insensitive to $\kappa\nu_0$ and thus determined without ambiguity.

By way of example, Figure 9b provides clear evidence for a K^+-induced increase in slope and a corresponding decrease in intercept for riboswitch folding data between 1 and 10 mM K^+, which reveals that the U → TS reaction becomes significantly more exothermic ($+\Delta\Delta H^{U\text{-}‡} = -8(2)$ kcal/mol) and yet also suffers from an increased entropic penalty ($\Delta\Delta S^{U\text{-}‡} = -27(6)$ cal/mol·K) with increasing [K^+]. By way of contrast, the corresponding thermodynamics from the transition to folded state (TS → F) reaction path (Figure 9c) reveals much smaller changes in enthalpy release ($+\Delta\Delta H^{‡\text{-}F} = -3.5(5)$ kcal/mol), accompanied by a considerable decrease in entropy ($\Delta\Delta S^{‡\text{-}F} = -10(1)$ kcal/mol·K) with increasing [K^+]. Altogether, the thermodynamics signal a major enthalpic benefit to folding at higher K^+ concentration in the folding (U → TS) reaction, while the predominant effect of increased K^+ in the unfolding (TS → F) direction is an increase in entropic penalty.

As the most dramatic changes in k_{fold} and k_{unfold} occur over the low-[K^+] range (see Figure 8), we summarize in Figure 10 the overall (a) free energy, (b) enthalpic, and (c) entropic landscapes for riboswitch folding between 1 and 10 mM K^+,

https://doi.org/10.1021/acs.jpcb.3c00245
J. Phys. Chem. B 2023, 127, 2430−2440

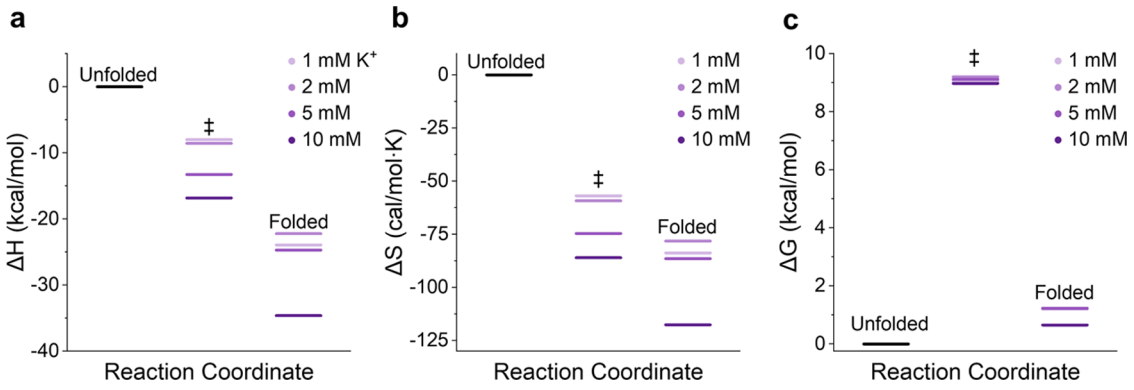

Figure 10. Energetic landscapes for the folding reaction at $[K^+]$ = 1, 2, 5, and 10 mM. (a) ΔH is negative (exothermic) over the entire reaction coordinate, decreasing between U → ‡ and ‡ → F states and becoming even more exothermic with higher $[K^+]$. (b) ΔS is also negative (entropically costly) throughout the folding reaction and becomes even more costly at higher $[K^+]$. (c) ΔG (300 K) reveals a large transition state barrier to folding/unfolding (U/F → ‡) despite a comparatively modest overall ΔG^0 (U → F). An increase in $[K^+]$ decreases both $\Delta G^{\ddagger}$ and ΔG°.

with the complete set of fitted data presented in SI Table 3. In agreement with previous work,[54] Figure 10 confirms the competition between enthalpic benefit ($\Delta H < 0$) and entropic cost ($-T\Delta S > 0$) in achieving both the transition and folded state conformations, specifically counterbalancing each other to generate large free energy barriers (≈10 kcal/mol) in the transition state region, yet for only a relatively modest (≈1 kcal/mol) overall folding ΔG°. Furthermore, the landscapes reveal that the formation of the transition and fully folded riboswitch states become noticeably more exothermic ($\Delta\Delta H^{U\text{-}\ddagger} < 0$; $\Delta\Delta H^{\circ} < 0$) and entropically costly ($-T\Delta\Delta S^{U\text{-}\ddagger} > 0$; $-T\Delta\Delta S^{\circ} > 0$) with increasing K^+. In terms of overall free energy, however, the transition state barrier decreases only slightly ($\Delta\Delta G^{U\text{-}\ddagger} < 0$) with $[K^+]$, as does free energy of the total overall folding process ($\Delta\Delta G^{\circ} < 0$). Interpretations of these thermodynamic and kinetic results are considered below.

4. DISCUSSION

4.1. Potassium-Mediated Bonding between Lysine and the Riboswitch Reflected in Kinetic and Thermodynamic Behavior. Increased exothermicity and entropic cost to folding are consistent with a physical picture in which K^+ acts as a bridge between lysine and the riboswitch binding pocket. The lysine riboswitch successfully folds even in the absence of potassium cations, but this pathway exhibits a much-reduced binding affinity between the ligand and RNA, due ostensibly to the carboxylic acid group not being able to bind in close proximity to the phosphate backbone. K^+ is therefore taken up into the riboswitch, lowering Coulomb repulsion, allowing for greater bonding interaction between lysine and the binding pocket, and thereby achieving more enthalpic release ($\Delta\Delta H^{\circ} < 0$). This effect can be compared to previous work that shows potassium drives folding in the RNA GAAA tetraloop receptor but may decrease exothermicity,[65] though helical packing that relies on GAAA tetraloop-receptor folding may still be enthalpically enhanced by potassium.[66] One plausible corollary is that any additional rigidity provided by lysine binding to the riboswitch pocket is itself the origin of the entropic barrier that grows with increasing potassium concentration (see Figure 10). Each of the lysine moieties is bound directly to the riboswitch or via a bridging species such as water or potassium, creating a tight restriction that encapsulates lysine and allows the riboswitch to discriminate against other similar molecules. However, as K^+ provides one such point of contact between lysine and the riboswitch, its omission introduces additional (too much) flexibility in the binding pocket, increasing the entropy. As K^+ concentration increases and is incorporated into the binding pocket, constraints on the orientation/position of lysine also increase and in so doing increase entropic penalties to folding. Although the riboswitch must be bound to lysine to fold and therefore achieve gene regulation, it is able to undergo these conformational changes with or without potassium. Interestingly, however, potassium stabilizes the folded state by both decreasing the unfolding rate (k_{unfold}) and increasing the folding rate (k_{fold}). This arises from potassium's thermodynamic role in the riboswitch binding pocket, where it forms part of the lysine site itself and therefore acts cooperatively as a second "ligand" controlling aptamer binding affinity.

4.2. Riboswitch Folding with Substitute Cations Less Effective at Promoting the Folded State. By way of a final set of studies, we explore the role of monovalent cationic size in impacting the lysine dissociation constant and folding rates. Indeed, previous studies have suggested that the lysine riboswitch can forgo the K^+ cation (ionic radius = 1.38 Å; V = 11.0 Å^3) for the much larger Cs^+ cation (ionic radius = 1.70 Å; V = 20.6 Å^3) to favor the folded riboswitch state,[48] but notably not the smaller Na^+ (ionic radius = 1.02 Å; V = 4.45 Å^3).[67] We therefore have reinvestigated the kinetics of riboswitch folding in the absence of K^+, instead utilizing Cs^+ or Na^+ to probe the extent to which potassium is replaceable or whether it is uniquely suited to its role in promoting folding. Cesium cation concentration dependence studies in Figure 11a reveal k_{fold} to be remarkably insensitive to cesium, while k_{unfold} decreases notably with increased $[Cs^+]$. This behavior would be consistent with a conformational selection (CS) mechanism, in which the riboswitch folds prior to the association of the Cs^+, and for which Cs^+ would need to be released before the riboswitch can unfold. Such kinetic competition for folded, cesium-unbound state (F + Cs^+ → U + Cs^+ vs F + Cs^+ → F·Cs^+) results in an increase in folded state dwell times and therefore K_{eq}. However, it is useful to point out that cesium is overall less effective at promoting riboswitch folding than K^+ due to the fact that potassium interacts with the riboswitch via both conformational selection and induced-fit type pathways (Figure 7, front face). The more rapid decrease in the unfolding rate constant (k_{unfold}) with K^+ vs Cs^+, as well as an increase in folding rate constant (k_{fold}) with K^+ implies that the

https://doi.org/10.1021/acs.jpcb.3c00245
J. Phys. Chem. B 2023, 127, 2430−2440

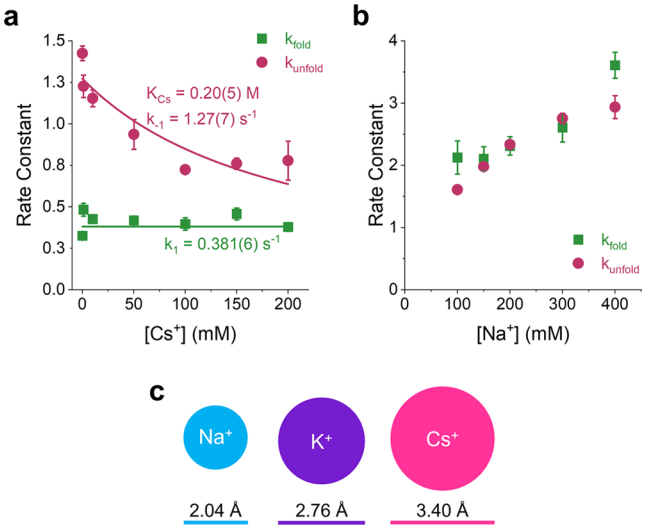

Figure 11. Cesium and sodium dependence on riboswitch folding (green squares) and unfolding (pink circles) rate constants. (a) [Cs^+] data series shows no cesium dependence on k_{fold} but a decrease in k_{unfold} with cesium concentration, which is indicative of a conformational selection folding mechanism. (b) [Na^+] data series shows increasing k_{fold} and k_{unfold} with sodium concentration, which points to the general association of Na^+ with the riboswitch, supporting the negatively charged RNA in both conformations. (c), relative Pauling-type crystal ionic diameters[67] of Na^+ (2.04 Å), K^+ (2.76 Å), and Cs^+ (3.40 Å).

binding pocket, while tolerant of a slightly larger cation such as Cs^+, is nevertheless more suited to K^+ for cationic control of riboswitch folding.

By way of comparison, we also examine why Na^+ is found to be a poor substitute[48] for K^+ by measuring the riboswitch folding/unfolding rate constants as a function of additional [Na^+] (see Figure 11b). The unfolding rate constant rises, possibly toward saturation, while the folding rate constant steadily grows with increasing [Na^+], behavior which is kinetically inconsistent with either a conformational selection (CS), induced fit (IF), or a hybrid binding model. Indeed, such an increase in both k_{fold} and k_{unfold} with Na^+ suggests an altogether different kind of interaction between the cation and the riboswitch, one in which sodium is not included in the binding site that both potassium and cesium can apparently occupy. Instead, as in Manning counterion condensation theory,[65,68,69] the Na^+ atmosphere may simply act to reduce overall Coulombic repulsion between the negatively charged riboswitch backbone, in which case additional sodium helps stabilize the transition state and therefore increases both k_{fold} and k_{unfold}.

The different behaviors between the three monovalent species in relation to the lysine riboswitch demonstrate that potassium appears uniquely suited to forming part of the lysine binding site, while sodium and cesium may be inadequate substitutes due to size (see Figure 11c for relative cationic radii of Na^+, K^+, and Cs^+). The binding pocket of the riboswitch is tailored to fit lysine and K^+; consequently, sodium ions may be too small to create the right fit between lysine and the riboswitch, which would allow them to bind and unbind easily without fully bridging the lysine and RNA. Conversely, the cesium may be too large and may block or distort parts of the binding pocket critical to lysine recognition, preventing lysine from binding to the RNA or binding in an entirely different position, each of which could inhibit appropriate lysine binding and subsequent riboswitch folding.

5. CONCLUSIONS

We have investigated the role of K^+ cations in the folding of the *B. subtilis* lysine riboswitch with temperature-dependent single-molecule kinetic and thermodynamic studies. The results reveal that although potassium is not strictly required for riboswitch folding, it operates synergistically with lysine to stabilize the folded state under physiological salt conditions. As the concentration of potassium increases, the riboswitch affinity for lysine increases (K_{Lys} decreases), the folding rate (k_{fold}) increases, and the unfolding rate (k_{unfold}) decreases, with potassium promoting a more enthalpically favored ($\Delta H < 0$) and rigid ($-T\Delta S > 0$) binding pocket. Consequently, an increase in potassium concentration is accompanied by greater exothermicity in the folding reaction due to stronger bonding between lysine, potassium, and RNA, as well as an increased entropic barrier to folding, resulting from greater constraints on lysine and the binding pocket.

Furthermore, we have studied the thermodynamics of larger/smaller monovalent ions in replacing potassium-assisted riboswitch folding. The studies indicate that while Cs^+ promotes the folding of the lysine riboswitch via a conformational selection (CS) mechanism, Na^+ does not appear to interact directly with the binding pocket and stabilizes the riboswitch RNA backbone in both the folded and unfolded state. Potassium is found to be well adapted to encourage folding, presumably because its size allows it to properly bridge bonding between lysine and the riboswitch without blocking other bonding interactions. This could be particularly interesting as it offers an opportunity for cationic control of riboswitch gene regulation activity by changing [K^+], which could be important in tuning riboswitch responsivity to lysine analogues.

■ ASSOCIATED CONTENT

Supporting Information

The Supporting Information is available free of charge at https://pubs.acs.org/doi/10.1021/acs.jpcb.3c00245.

Derivation of the steady-state kinetic analysis expressions; and summary tables for all thermodynamic quantities obtained from this work (PDF)

■ AUTHOR INFORMATION

Corresponding Author

David J. Nesbitt − *JILA, University of Colorado Boulder and National Institute of Standards and Technology, Boulder, Colorado 80309, United States; Department of Chemistry, University of Colorado Boulder, Boulder, Colorado 80309, United States; Department of Physics, University of Colorado Boulder, Boulder, Colorado 80309, United States;* orcid.org/0000-0001-5365-1120; Email: djn@jila.colorado.edu

Author

Andrea Marton Menendez − *JILA, University of Colorado Boulder and National Institute of Standards and Technology, Boulder, Colorado 80309, United States; Department of Chemistry, University of Colorado Boulder, Boulder, Colorado 80309, United States*

Complete contact information is available at:

https://pubs.acs.org/10.1021/acs.jpcb.3c00245

Notes

The authors declare no competing financial interest.

■ ACKNOWLEDGMENTS

Initial support for this work has been through the National Science Foundation under grants CHE 1665271/2053117 from the Chemical, Structure, Dynamics, and Mechanisms-A Program, with recent transition support from the Air Force Office of Scientific Research (FA9550-15-1-0090) and additional funds for the development of the confocal apparatus from PHY-1734006 (Physics Frontier Center Program). We would also like to acknowledge early seed contributions by the W. M. Keck Foundation Initiative in RNA Sciences at the University of Colorado, Boulder.

■ REFERENCES

(1) Serganov, A.; Patel, D. J. Molecular recognition and function of riboswitches. *Curr. Opin. Struct. Biol.* **2012**, *22*, 279−286.
(2) Garst, A. D.; Edwards, A. L.; Batey, R. T. Riboswitches: Structures and mechanisms. *Cold Spring Harbor Perspect. Biol.* **2011**, *3*, No. a003533.
(3) Serganov, A. The long and the short of riboswitches. *Curr. Opin. Struct. Biol.* **2009**, *19*, 251−259.
(4) Breaker, R. R. Riboswitches and the RNA world. *Cold Spring Harbor Perspect. Biol.* **2012**, *4*, No. a003566.
(5) Lemay, J. F.; Desnoyers, G.; Blouin, S.; Heppell, B.; Bastet, L.; St-Pierre, P.; Massé, E.; Lafontaine, D. A. Comparative study between transcriptionally- and translationally-acting adenine riboswitches reveals key differences in riboswitch regulatory mechanisms. *PLoS Genet.* **2011**, *7*, No. e1001278.
(6) Jones, C. P.; Ferre-D'Amare, A. R. Long-range interactions in riboswitch control of gene expression. *Ann. Rev. Biophys.* **2017**, *46*, 455−481.
(7) Dambach, M.; Sandoval, M.; Updegrove, T. B.; Anantharaman, V.; Aravind, L.; Waters, L. S.; Storz, G. The ubiquitous yybP-ykoY riboswitch is a manganese-responsive regulatory element. *Mol. Cell* **2015**, *57*, 1099−1109.
(8) Furukawa, K.; Ramesh, A.; Zhou, Z.; Weinberg, Z.; Vallery, T.; Winkler, W. C.; Breaker, R. R. Bacterial riboswitches cooperatively bind Ni^{2+} or Co^{2+} ions and control expression of heavy metal transporters. *Mol. Cell* **2015**, *57*, 1088−1098.
(9) Batey, R. T.; Gilbert, S. D.; Montange, R. K. Structure of a natural guanine-responsive riboswitch complexed with the metabolite hypoxanthine. *Nature* **2004**, *432*, 411−415.
(10) Trausch, J. J.; Xu, Z.; Edwards, A. L.; Reyes, F. E.; Ross, P. E.; Knight, R.; Batey, R. T. Structural basis for diversity in the SAM clan of riboswitches. *Proc. Nat. Acad. Sci. U.S.A.* **2014**, *111*, 6624−6629.
(11) Ren, A.; Rajashankar, K. R.; Patel, D. J. Fluoride ion encapsulation by Mg^{2+} ions and phosphates in a fluoride riboswitch. *Nature* **2012**, *486*, 85−89.
(12) Montange, R. K.; Mondragón, E.; van Tyne, D.; Garst, A. D.; Ceres, P.; Batey, R. T. Discrimination between closely related cellular metabolites by the SAM-I riboswitch. *J. Mol. Biol.* **2010**, *396*, 761−772.
(13) Polaski, J. T.; Webster, S. M.; Johnson, J. E., Jr.; Batey, R. T. Cobalamin riboswitches exhibit a broad range of ability to discriminate between methylcobalamin and adenosylcobalamin. *J. Biol. Chem.* **2017**, *292*, 11650−11658.
(14) Mandal, M.; Boese, B.; Barrick, J. E.; Winkler, W. C.; Breaker, R. R. Riboswitches control fundamental biochemical pathways in bacillus subtilis and other bacteria. *Cell* **2003**, *113*, 577−586.
(15) Croft, M. T.; Moulin, M.; Webb, M. E.; Smith, A. G. Thiamine biosynthesis in algae is regulated by riboswitches. *Proc. Nat. Acad. Sci. U.S.A.* **2007**, *104*, 20770−20775.
(16) Nguyen, G. T. D. T.; Scaife, M. A.; Helliwell, K. E.; Smith, A. G. Role of riboswitches in gene regulation and their potential for algal biotechnology. *J. Phycol.* **2016**, *52*, 320−328.
(17) Warner, K. D.; Homan, P.; Weeks, K. M.; Smith, A. G.; Abell, C.; Ferré-D'Amaré, A. R. Validating fragment-based drug discovery for biological RNAs: Lead fragments bind and remodel the TPP riboswitch specifically. *Chem. Biol.* **2014**, *21*, 591−595.
(18) Blount, K. F.; Breaker, R. R. Riboswitches as antibacterial drug targets. *Nat. Biotechnol.* **2006**, *24*, 1558−1564.
(19) Hallberg, Z. F.; Su, Y.; Kitto, R. Z.; Hammond, M. C. Engineering and in vivo applications of riboswitches. *Ann. Rev. Biochem.* **2017**, *86*, 515−539.
(20) Sabet, F. S.; Hosseini, M.; Khabbaz, H.; Dadmehr, M.; Ganjali, M. R. FRET-based aptamer biosensor for selective and sensitive detection of aflatoxin B1 in peanut and rice. *Food Chem.* **2017**, *220*, 527−532.
(21) Trausch, J. J.; Ceres, P.; Reyes, F. E.; Batey, R. T. The structure of a tetrahydrofolate-sensing riboswitch reveals two ligand binding sites in a single aptamer. *Structure* **2011**, *19*, 1413−1423.
(22) Gao, A.; Serganov, A. Structural insights into recognition of c-di-AMP by the ydaO riboswitch. *Nat. Chem. Biol.* **2014**, *10*, 787−792.
(23) Poiata, E.; Meyer, M. M.; Ames, T. D.; Breaker, R. R. A variant riboswitch aptamer class for s-adenosylmethionine common in marine bacteria. *RNA* **2009**, *15*, 2046−2056.
(24) Mandal, M.; Lee, M.; Barrick, J. E.; Weinberg, Z.; Emilsson, G. M.; Ruzzo, W. L.; Breaker, R. R. A glycine-dependent riboswitch that uses cooperative binding to control gene expression. *Science* **2004**, *306*, 275−279.
(25) Butler, E. B.; Xiong, Y.; Wang, J. M.; Strobel, S. A. Structural basis of cooperative ligand binding by the glycine riboswitch. *Chem. Biol.* **2011**, *18*, 293−298.
(26) Huang, L. L.; Serganov, A.; Patel, D. J. Structural insights into ligand recognition by a sensing domain of the cooperative glycine riboswitch. *Mol. Cell* **2010**, *40*, 774−786.
(27) Hennelly, S. P.; Novikova, I. V.; Sanbonmatsu, K. Y. The expression platform and the aptamer: Cooperativity between Mg^{2+} and ligand in the SAM-I riboswitch. *Nucleic Acids Res.* **2013**, *41*, 1922−1935.
(28) Choudhary, P. K.; Sigel, R. K. O. Mg^{2+}-induced conformational changes in the btuB riboswitch from E. coli. *RNA* **2014**, *20*, 36−45.
(29) Hyde, J.; Braisted, A. C.; Randal, M.; Arkin, M. R. Discovery and characterization of cooperative ligand binding in the adaptive region of interleukin-2. *Biochemistry* **2003**, *42*, 6475−6483.
(30) Ascenzi, P.; Bocedi, A.; Bolli, A.; Fasano, M.; Notari, S.; Polticelli, F. Allosteric modulation of monomeric proteins. *Biochem. Mol. Biol. Edu.* **2005**, *33*, 169−176.
(31) Laskowski, R. A.; Gerick, F.; Thornton, J. M. The structural basis of allosteric regulation in proteins. *FEBS Lett.* **2009**, *583*, 1692−1698.
(32) Jaffe, E. K. Morpheeins − a new structural paradigm for allosteric regulation. *Trends Biochem. Sci.* **2005**, *30*, 490−497.
(33) Jose, A. M.; Soukup, G. A.; Breaker, R. R. Cooperative binding of effecters by an allosteric ribozyme. *Nucleic Acids Res.* **2001**, *29*, 1631−1637.
(34) Çetinkol, Ö. P.; Hud, N. V. Molecular recognition of poly(a) by small ligands: An alternative method of analysis reveals nanomolar, cooperative and shape-selective binding. *Nucleic Acids Res.* **2009**, *37*, 611−621.
(35) Ramisetty, S. R.; Baranger, A. M. Cooperative binding of a quinoline derivative to an RNA stem loop containing a dangling end. *Bioorg. Med. Chem. Lett.* **2010**, *20*, 3134−3137.
(36) Lifschitz, A. M.; Young, R. M.; Mendez-Arroyo, J.; McGuirk, C. M.; Wasielewski, M. R.; Mirkin, C. A. Cooperative electronic and structural regulation in a bioinspired allosteric photoredox catalyst. *Inorg. Chem.* **2016**, *55*, 8301−8308.
(37) Scarso, A.; Scheffer, U.; Gobel, M.; Broxterman, Q. B.; Kaptein, B.; Formaggio, F.; Toniolo, C.; Scrimin, P. A peptide template as an allosteric supramolecular catalyst for the cleavage of phosphate esters. *Proc. Nat. Acad. Sci. U.S.A.* **2002**, *99*, 5144−5149.

(38) Fastrez, J. Engineering allosteric regulation into biological catalysts. *ChemBioChem* **2009**, *10*, 2824−2835.
(39) Perutz, M. F. Stereochemistry of cooperative effects in haemoglobin: Haem−haem interaction and the problem of allostery. *Nature* **1970**, *228*, 726−734.
(40) Yoon, H. J.; Kuwabara, J.; Kim, J. H.; Mirkin, C. A. Allosteric supramolecular triple-layer catalysts. *Science* **2010**, *330*, 66−69.
(41) Peselis, A.; Serganov, A. Cooperativity and allostery in RNA systems In *Allostery: Methods and Protocols*; DiPaola, L.; Giuliani, A., Eds.; Springer Nature, 2021; Vol. *2253*, pp 255−271.
(42) Tsai, C.-J.; del Sol, A.; Nussinov, R. Protein allostery, signal transmission and dynamics: A classification scheme of allosteric mechanisms. *Mol. Biosyst.* **2009**, *5*, 207−216.
(43) Joly, J. P.; Mata, G.; Eldin, P.; Briant, L.; Fontaine-Vive, F.; Duca, M.; Benhida, R. Artificial nucleobase-amino acid conjugates: A new class of tar RNA binding agents. *Chem. - Eur. J.* **2014**, *20*, 2071−2079.
(44) Cossins, B. P.; Lawson, A. D. G. Small molecule targeting of protein-protein interactions through allosteric modulation of dynamics. *Molecules* **2015**, *20*, 16435−16445.
(45) Chatzigoulas, A.; Cournia, Z. Rational design of allosteric modulators: Challenges and successes. *WIREs Comput. Mol. Biosci.* **2021**, *11*, No. e1529.
(46) Barrick, J. E.; Breaker, R. R. The distributions, mechanisms, and structures of metabolite-binding riboswitches. *Genome Biol.* **2007**, *8*, No. R239.
(47) Garst, A. D.; Héroux, A.; Rambo, R. P.; Batey, R. T. Crystal structure of the lysine riboswitch regulatory mRNA element. *J. Biol. Chem.* **2008**, *283*, 22347−22351.
(48) Serganov, A.; Huang, L.; Patel, D. J. Structural insights into amino acid binding and gene control by a lysine riboswitch. *Nature* **2008**, *455*, 1263−1267.
(49) Blouin, S.; Lafontaine, D. A. A loop loop interaction and a K-turn motif located in the lysine aptamer domain are important for the riboswitch gene regulation control. *RNA* **2007**, *13*, 1256−1267.
(50) Blouin, S.; Chinnappan, R.; Lafontaine, D. A. Folding of the lysine riboswitch: Importance of peripheral elements for transcriptional regulation. *Nucl. Acids Res.* **2011**, *39*, 3373−3387.
(51) Fiegland, L. R.; Garst, A. D.; Batey, R. T.; Nesbitt, D. J. Single-molecule studies of the lysine riboswitch reveal effector-dependent conformational dynamics of the aptamer domain. *Biochemistry* **2012**, *51*, 9223−9233.
(52) Sung, H.-L.; Nesbitt, D. J. High pressure single-molecule FRET studies of the lysine riboswitch: Cationic and osmolytic effects on pressure induced denaturation. *Phys. Chem. Chem. Phys.* **2020**, *22*, 15853−15866.
(53) Smith-Peter, E.; Lamontagne, A. M.; Lafontaine, D. A. Role of lysine binding residues in the global folding of the lysC riboswitch. *RNA Biol.* **2015**, *12*, 1372−1382.
(54) Marton Menendez, A.; Nesbitt, D. J. Lysine-dependent entropy effects in the B. subtilis lysine riboswitch: Insights from single-molecule thermodynamic studies. *J. Phys. Chem. B* **2022**, *126*, 69−79.
(55) Hammes, G. G.; Chang, Y.-C.; Oas, T. G. Conformational selection or induced fit: A flux description of reaction mechanism. *Proc. Nat. Acad. Sci. U.S.A.* **2009**, *106*, 13737−13741.
(56) Scarso, A.; Zaupa, G.; Houillon, F. B.; Prins, L. J.; Scrimin, P. Tripodal, cooperative, and allosteric transphosphorylation metallocatalysts. *J. Org. Chem.* **2007**, *72*, 376−385.
(57) Fiore, J. L.; Holmstrom, E. D.; Nesbitt, D. J. Entropic origin of Mg^{2+}-facilitated RNA folding. *Proc. Nat. Acad. Sci. U.S.A.* **2012**, *109*, 2902−2907.
(58) Sengupta, A.; Sung, H.-L.; Nesbitt, D. J. Amino acid specific effects on RNA tertiary interactions: Single-molecule kinetic and thermodynamic studies. *J. Phys. Chem. B* **2016**, *120*, 10615−10627.
(59) Nicholson, D. A.; Sengupta, A.; Sung, H. L.; Nesbitt, D. J. Amino acid stabilization of nucleic acid secondary structure: Kinetic insights from single-molecule studies. *J. Phys. Chem. B* **2018**, *122*, 9869−9876.
(60) Nicholson, D. A.; Sengupta, A.; Nesbitt, D. J. Chirality-dependent amino acid modulation of RNA folding. *J. Phys. Chem. B* **2020**, *124*, 11561−11572.
(61) Kinz-Thompson, C. D.; Bailey, N. A.; Gonzalez, R. L., Jr.Precisely and Accurately Inferring Single-Molecule Rate Constants. In *Methods in Enzymology*; Elsevier 2016; Vol. *581*, pp 187−225.
(62) Holmstrom, E. D.; Nesbitt, D. J. Biophysical insights from temperature-dependent single-molecule Förster resonance energy transfer. *Annu. Rev. Phys. Chem.* **2016**, *67*, 441−465.
(63) Zwanzig, R.; Szabo, A.; Bagchi, B. Levinthal's paradox. *Proc. Nat. Acad. Sci. U.S.A.* **1992**, *89*, 20−22.
(64) Best, R. B.; Hummer, G. Diffusive model of protein folding dynamics with Kramers turnover in rate. *Phys. Rev. Lett.* **2006**, *96*, No. 228104.
(65) Holmstrom, E. D.; Fiore, J. L.; Nesbitt, D. J. Thermodynamic origins of monovalent facilitated RNA folding. *Biochemistry* **2012**, *51*, 3732−3743.
(66) Vander Meulen, K. A.; Butcher, S. E. Characterization of the kinetic and thermodynamic landscape of RNA folding using a novel application of isothermal titration calorimetry. *Nucleic Acids Res.* **2012**, *40*, 2140−2151.
(67) Marcus, Y. Ionic radii in aqueous solutions. *Chem. Rev.* **1988**, *88*, 1475−1498.
(68) Sharp, K. A.; Friedman, R. A.; Misra, V.; Hecht, J.; Honig, B. Salt effects on polyelectrolyte−ligand binding: Comparison of poisson−boltzmann, and limiting law/counterion binding models. *Biopolymers* **1995**, *36*, 245−262.
(69) Manning, G. S. Limiting laws and counterion condensation in polyelectrolyte solutions I. Colligative properties. *J. Chem. Phys.* **1969**, *51*, 924−933.

https://doi.org/10.1021/acs.jpcb.3c00245
J. Phys. Chem. B 2023, 127, 2430−2440